equation has just deomonstrated the equality

$$\langle\eta_0^{(j)}|(\mathbf{v}^j)_\alpha=(\mu hc^2/\lambda_\alpha)\langle\eta_{1\alpha}^{(j)}|\,.$$

A typical term of $\langle\eta_{1\alpha}^{(j)}|n^{*(j)}\rangle$ is

$$\langle\eta_0^{(j)}|v_\alpha^{(j)}(\partial/\partial x_\alpha)n^{(j)*}\rangle=(\mu/k_BT)(\partial/\partial x_\alpha)Q_\alpha^{(j)}\,. \quad \text{(C19)}$$

Similarly, as in (A8),

$$\sum_j\langle\eta_0^{(j)}|n^*\rangle=(\mu/k_BT)\epsilon_T\,. \quad \text{(C20)}$$

Thus, taking $\langle\eta_0^{(j)}|$ on the jth Boltzmann equation and summing over j yields

$$(\partial\epsilon_T/\partial t)+\nabla\cdot\mathbf{Q}=0\,. \quad \text{(C21)}$$

We conclude that the presence of several isotropic and dispersionless branches does not modify the essential physical conclusion reached in our main discussion. Dispersion and anisotropy would indeed complicate the details.

PHYSICAL REVIEW VOLUME 148, NUMBER 2 12 AUGUST 1966

Thermal Conductivity, Second Sound, and Phonon Hydrodynamic Phenomena in Nonmetallic Crystals*

R. A. GUYER
Department of Physics, Duke University, Durham, North Carolina
AND
J. A. KRUMHANSL
Laboratory of Atomic and Solid State Physics, Cornell University, Ithaca, New York

(Received 27 December 1965; revised manuscript received 17 March 1966)

A variety of phonon-gas phenomena in nonmetals are discussed in a unified manner using a set of macroscopic equations developed from the solution of the linearized phonon Boltzmann equation. This set of macroscopic equations, appropriate for the description of a low-temperature phonon gas, is solved for a cylindrical sample in the limit $\lambda_N\ll R$; $\lambda_N\lambda_R^{\varepsilon}\gg R^2$. Here λ_N is the normal-process mean free path, λ_R^{ε} is the mean free path for momentum-loss scattering calculated in the Ziman limit, and R is the radius of the sample. The solution in this limit exhibits Poiseuille flow of the phonon gas as first discussed by Sussmann and Thellung. An equation for the thermal conductivity which correctly includes this phenomenon is found. Using this equation, the possible outcomes of steady-state thermal-conductivity measurements are discussed in terms of the microscopic scattering rates. Heat-pulse propagation is discussed from a similar point of view. The existence of Poiseuille flow in steady-state thermal-conductivity measurements bears directly on the possibility of observing second sound in solids. A quantitative analysis of available data on LiF suggests that the chemical purity of these samples sets very stringent limits on the observation of either of these effects. The observation of Poiseuille flow in solid He^4 samples by Mezov-Deglin strongly suggests that this material is a prime subject for investigations of second-sound propagation.

I. INTRODUCTION

IN a perfect single crystal of dielectric solid the phonons undergo two distinctly different kinds of scattering processes, normal processes (N-processes) in which quasimomentum is conserved and umklapp processes (U-processes) in which it is not.[1] As the temperature of the solid is varied the relative rate of these scattering processes changes drastically with an attending change in the transport properties involving phonons in the solid. The presence in thermal conductivity of a Ziman limit,[2] and the possibilities of Poiseuille flow[3,4] and the second sound[5–7] in a phonon gas are consequences of these changes. The purpose of this paper is to discuss the entire spectrum of possible low-temperature behavior of a phonon gas from a single unified point of view.

The starting point of the analysis is the system of macroscopic equations derived in the previous paper.[8] These equations describe the time- and space-dependent behavior of a phonon gas; they are set down in Sec. II. Two sets of equations valid in opposite limits (deter-

* This work was supported in part by the Army Research Office (Durham), the National Science Foundation, the Office of Naval Research, and the U. S. Atomic Energy Commission (NYO-2391-32).

[1] R. E. Peierls, Ann. Physik. 3, 1055 (1929). Throughout the text we use the phrase "U processes" to refer to the case when umklapp scattering alone occurs. Otherwise we use "R processes" to refer to the case when a number of resistive scattering mechanisms are operating in the sample.

[2] J. M. Ziman, *Electrons and Phonons* (Oxford University Press, New York, 1960), Chap. 7.

[3] J. A. Sussmann and A. Thellung, Proc. Phys. Soc. (London) 81, 1122 (1963).

[4] R. N. Gurzi, Zh. Eksperim. i Teor. Fiz. 46, 719 (1964) [English transl.: Soviet Phys.—JETP 19, 490 (1964)].

[5] J. C. Ward and J. Wilks, Phil. Mag. 43, 48 (1952).

[6] E. W. Prohofsky and J. A. Krumhansl, Phys. Rev. 133, 1403 (1964).

[7] R. A. Guyer and J. A. Krumhansl, Phys. Rev. 133, 1411 (1964).

[8] The previous [Phys. Rev. 148, 766 (1966)] paper is hereafter referred to as I; the equations from the paper are denoted by I(—). (The need for symmetrization and the particular choice of basis is discussed.)

mined by the relative rates of N-processes and R-processes) are required. In Sec. III these equations are applied to a discussion of steady-state thermal conductivity which generalizes the results obtained in I to cover spatially nonuniform heat flow. This leads to the incorporation of "Poiseuille flow" (Sec. IV) of the phonon gas into an equation for the lattice thermal conductivity, thus generalizing Eq. I(44) of the previous paper (Sec. V). In Sec. VI the equations for time-dependent phenomena are reviewed and then in Sec. VII we discuss how all of these are interrelated. Included are: (1) the various experiments which can be done on a phonon gas, (2) the microscopic scattering rates which determine where (in temperature and frequency) these experiments should be done, (3) the fundamental quantities which can be extracted from the measurements in each experiment, and the (4) the present experimental situation with respect to each experiment. In Sec. VIII we discuss the current situation for solid He^4 and LiF. In an Appendix we show the relation of the system of macroscopic equations we have obtained to those that follow from the Callaway equation.[9]

II. MACROSCOPIC EQUATIONS

In I we showed that in an isotropic-dispersionless phonon gas when the R-processes are relatively rapid compared to the N-processes, a_0 and $\mathbf{a}_1$ obey the equations,

$$\partial a_0/\partial t+\langle 0|\mathbf{c}\cdot\nabla|1\rangle\mathbf{a}_1=0, \tag{1a}$$

and

$$\mathbf{a}_1-\langle 1|\mathbf{R}^{*-1}|1\rangle\langle 1|\mathbf{c}\cdot\nabla|0\rangle a_0=0. \tag{1b}$$

These equations are equivalent to I(22a) and I(33), but we briefly restate the physical ideas and meaning of the notation. In I the solution of the linearized phonon Boltzmann equation was developed by expanding the the phonon distribution function in terms of a set of functions, $\{\eta_\nu^*(\mathbf{q})\}$, in phonon wave-number space, $\mathbf{q}$ space. The coefficients a_0, $\mathbf{a}_1$, $\cdots$ depend upon position $\mathbf{x}$ and time t. The $\mathbf{q}$-space functions are defined in Appendix I.A; particular among them are

$$|\eta_0^*\rangle=|0\rangle=\mu x(2\sinh x)^{-1},$$
$$|\eta_{1z}^*\rangle=|1z\rangle=(\lambda_z q_z/k_BT)(2\sinh x)^{-1},$$

where $x=\hbar\omega/k_BT$, μ and λ_z are normalization constants, and the $\mathbf{q}$ dependence enters through $\hbar\omega(\mathbf{q})$ as well as explicitly. Linear-vector-space notation is employed in an apparent manner; for example the scalar product

$$\langle 0||z\rangle=\int_{\text{B.Z.}} d\mathbf{q}\,\mu x(2\sinh\tfrac{1}{2}x)^{-1}(\lambda_z q_z/k_BT)(2\sinh\tfrac{1}{2}x)^{-1}.$$

Rearrangement of the hyperbolic functions will show that in fact these scalar products are identical to the integrals over the phonon distribution usually encountered in phonon calculations.

The meaning of the other quantities in Eqs. (1a) and (1b) is as follows: $\mathbf{c}=c\mathbf{q}/|\mathbf{q}|$ is the velocity of the phonons; the acoustic approximation is used throughout this paper. The space- and time-dependent coefficients a_0 and $\mathbf{a}_1$ are proportional to the deviation, ϵ_T, of the local energy density from thermal equilibrium and to the heat current, Q, respectively[10];

$$a_0=(\mu/k_BT)\epsilon_T,$$
$$a_{1\alpha}=(\lambda_\alpha/k_BT\hbar c^2)Q_\alpha,\quad \alpha=x,y,z,$$

where Q_α is the heat current carried in the α direction. Equation (1a) is the statement of energy conservation; Eq. (1b) is a generalized thermal-conductivity equation. [The same correspondence holds for Eqs. (2a) and (2b) below]. The operators $\mathbf{R}^*$ and $\mathbf{N}^*$ in Eq. (1b) and Eq. (2b) (below) are symmetrized linear-scattering operators for the R processes and the N processes, respectively.[8]

Since the equations are linear we frequently Fourier analyze the space- and time-dependent coefficients a_0, $\mathbf{a}_1$ in terms of $\exp i(\mathbf{k}\cdot\mathbf{x}-\Omega t)$. In this expression Ω is the frequency of oscillation of a macroscopic quantity, as determined experimentally, for example, by applying heat periodically with frequency Ω. Similarly, $\mathbf{k}$ refers to the macroscopic spatial distribution of temperature or heat current.

Equations (1a) and (1b) [also Eqs. (2a) and (2b) below] were derived in such a way that conservation conditions on collision operators are met exactly. At this point relaxation times may be introduced without fear of violating these important conditions. For Eqs. (1a) and (1b) to apply τ_R, the time which characterizes R-process scattering, must be the shortest microscopic collision time. Thus, for variation as $\exp i(\mathbf{k}\cdot\mathbf{x}-\Omega t)$, Eq. (1b) is correct up to terms of order $\Omega\tau_R$ i.e., it is valid in the regime $\Omega\tau_R\ll 1$.

When the N-processes are relatively rapid compared to the R-processes $\Omega\tau_N\ll 1$, and the time variation of a_0 and $\mathbf{a}_1$ is fast compared to the R-processes scattering rate, $\Omega\tau_R\ll 1$, a_0 and $\mathbf{a}_1$ satisfy different equations [I(56), (57)]

$$\partial a_0/\partial t+\langle 0|\mathbf{c}\cdot\nabla|1\rangle\mathbf{a}_1=0, \tag{2a}$$

$$\partial\mathbf{a}_1/\partial t+\langle 1|\mathbf{R}^*|1\rangle\mathbf{a}_1-\langle 0|\mathbf{c}\cdot\nabla|1\rangle a_0 -\langle 1|\mathbf{c}\cdot\nabla\mathbf{N}^{*-1}\mathbf{c}\cdot\nabla|1\rangle\mathbf{a}_1=0. \tag{2b}$$

In this limit τ_N, the time which characterizes the N-process scattering rate, is the shortest microscopic time; $\Omega\tau_N\ll 1$ is then the condition for a local thermal description. Equation (2b) is correct up to terms of order $\Omega\tau_N$ and $(\Omega\tau_R)^{-1}$. The intermediate range between

[9] J. Callaway, Phys. Rev. **113**, 1046 (1959). The phrase Callaway equation is used to refer to either the basic Boltzmann equation containing the Callaway form of the collision term [see Eq. (A1)] or to the final expression obtained from that equation for the thermal conductivity.

[10] For a temperature disturbance of the form $\exp i(\mathbf{k}\cdot\mathbf{x}-\Omega t)$, Ω measures the rate of variation in time of a thermodynamic quantity. It must be possible for equilibrium to take place during this time.

the two limits, ($\Omega\tau_R \ll 1$, $\tau_R \ll \tau_N$) and ($\Omega\tau_N \ll 1, \Omega\tau_R \ll 1$), cannot easily be treated with the Boltzmann equation as developed in I.

The Callaway method for treating the phonon Boltzmann equation has found use as an algebraically convenient way to include both limits in a single analysis. We therefore have re-examined its use for our present purposes. But as we show in the Appendix it leads to spurious terms which make its validity suspect in all but the limiting cases [for which Eqs. (1a) and (1b) and (2a) and (2b) are valid]. Hence we use the set of macroscopic Eqs. (1a) and (1b) and (2a) and (2b) in the appropriate limits and treat the intermediate region with the interpolation which we introduced in I, [I(44)]. The entire discussion in this paper is in this framework.

III. STEADY-STATE THERMAL TRANSPORT

In I we discussed steady-state thermal conductivity, $\kappa = \kappa(0,0)$, using Eqs. (1a) and (1b) and Eqs. (2a) and (2b) (the time-dependent terms are set equal to zero). It was found that Eqs. (1a) and (1b) yield an appropriate expression for κ in the limit that $\mathbf{R}^* \to +\infty$ and that Eqs. (2a) and (2b) yield an appropriate expression for κ in the opposite limit, $\mathbf{N}^* \to +\infty$, the Ziman limit. Consideration of how these two cases are added to yield a single expression for κ led to the idea of switching factors between the limiting expressions. These are functions of the relative rates of the two kinds of scattering processes. The choice of

$$s = \frac{\langle 1|\tau_N|1\rangle}{\langle 1|\tau_R{}^B|1\rangle} = \int_0^\infty \tau_N(x) x^4 \frac{e^x}{(e^x-1)^2} dx \Big/ \int_0^\infty \tau_R{}^B(x) x^4 \frac{e^x}{(e^x-1)^2} dx$$

in I(44) for the switching parameter yielded an equation for κ very much like the Callaway result[9] [see the discussion following Eq. (15) below].

The development given in I did not deal in an explicit manner with boundary effects. These are important experimentally so we now discuss them. Traditionally, in the very low-temperature limit the Casimir model[11,12] has been used to treat thermal conduction. In the context of the phonon-gas description this is equivalent to "Knudsen flow" or "ballistic transport" and is applicable when the bulk phonon mean free path[13] is large compared to the sample diameter.

On the other hand when the mean free path is significantly less than sample dimensions, Eqs. (1a) and (1b) and (2a) and (2b) give a correct description and their full hydrodynamic content must be explored. Conventional, spatially uniform, steady-state heat current is only one possible solution. An obvious generalization to be examined is steady "Poiseuille" flow, which we now discuss.

IV. POISEUILLE FLOW

Consider Eq. (2b) in the form[14]

$$[\langle 1|\mathbf{c}\cdot\nabla \mathbf{N}^{*-1}\mathbf{c}\cdot\nabla|1\rangle - \langle 1|\mathbf{R}^*|1\rangle] a_{1z} = -\langle 0|\mathbf{c}\cdot\nabla|1\rangle a_0.$$

The operators $\mathbf{N}^*$ and $\mathbf{R}^*$ are again identified with isotropic relaxation times $-\tau_N(\mathbf{q})$ and $-\tau_R(\mathbf{q})$. For the first term on the left-hand side of this equation we find

$$-\tfrac{1}{5}\tau_N[\nabla^2 + 2\nabla(\nabla\cdot\ )] a_{1z}. \tag{3}$$

This result follows from using the definition of the scalar product to write

$$\langle 1|\mathbf{c}\cdot\nabla \mathbf{N}^{*-1}\mathbf{c}\cdot\nabla|1\rangle = -\lambda_z{}^2 \frac{V}{(2\pi)^3}\int d\mathbf{q}\left(\frac{q_z}{k_B T}\right)^2 \frac{e^x}{(e^x-1)^2} \times[\tau_N(\mathbf{q})(\mathbf{c}\cdot\nabla)(\mathbf{c}\cdot\nabla)]$$

which can be reduced to the form

$$-\frac{\lambda_z{}^2}{\mu^2}\frac{1}{(\hbar c)^2}\langle 0|\tau_N|0\rangle \frac{1}{4\pi}\int_0^\pi \sin\theta d\theta \int_0^{2\pi} d\phi \times[\cos^2\theta(\mathbf{c}\cdot\nabla)(\mathbf{c}\cdot\nabla)],$$

where

$$\tau_N = \langle 0|\tau_N|0\rangle = \int_0^\infty \tau_N(x) x^4 \frac{e^x}{(e^x-1)^2} dx \Big/ \int_0^\infty x^4 \frac{e^x}{(e^x-1)^2} dx.$$

The angular integral in this equation yields

$$(1/15)c^2[\nabla^2 + 2\nabla(\nabla\cdot\ )].$$

From the normalization of $|0\rangle$ and $|1\rangle$ we have $\lambda_z{}^2/\hbar^2 c^2 \mu^2 = 3$. The combination of these results yields Eq. (3).

For the second term on the left-hand-side of Eq. (2b) (as written above) we have

$$\langle 1|\mathbf{R}^*|1\rangle = -\langle 1|\tau_R(\mathbf{q})^{-1}|1\rangle = -\langle 0|\tau_R(\mathbf{q})^{-1}|0\rangle,$$

where the second of these equalities follows from the isotropic nature of $\tau_R(\mathbf{q})$. Again from the definition of

[11] H. B. G. Casimir, Physica 5, 495 (1938).

[12] P. A. Carruthers, Rev. Mod. Phys. 33, 92 (1961). This paper also contains an excellent review of low-temperature thermal conductivity.

[13] For scattering from isotopic impurities or the anharmonic potential the scattering takes place continually throughout the bulk of the sample.

[14] We are concerned with one-dimensional heat flow and therefore specialize Eq. (2b) to this case. However, in calculating the matrix element which gives the operator on $\mathbf{a}_1$ in Eq. (2b) we do not specialize to one dimension. Hence, Eq. (4) may be generalized by replacing a_{1z} by $\mathbf{a}_1$.

$|0\rangle$ and the scalar product

$$\langle 1|\mathbf{R}^*|1\rangle = -\langle 0|\tau_R(\mathbf{q})^{-1}|0\rangle$$
$$= \int_0^\infty \tau_R(x)^{-1}x^4\frac{e^x}{(e^x-1)^2}dx \Big/ \int_0^\infty x^4\frac{e^x}{(e^x-1)^2}dx.$$

This average of the relaxation time rather than the relaxation time shall be referred to as the Ziman limit. Hence, we write $\langle 1|R^*|1\rangle = -\langle 0|\tau_R(\mathbf{q})^{-1}|0\rangle = -\tau_z^{-1}$.

These results are combined to write Eq. (2b) in the form

$$\nabla^2 a_{1z} + 2\nabla(\nabla\cdot a_{1z}) - \frac{a_{1z}}{\lambda^2} = 5\frac{\langle 0|\mathbf{c}\cdot\nabla|1\rangle}{\tau_N c^2}a_0, \qquad (4)$$

where $\lambda^2 = c^2\tau_N\tau_z/5$.

We may now solve the problem of steady-state heat current in a long cylindrical sample of radius R. When ∇a_0 and $\mathbf{a}_1$ have z components only, a_{1z} depends on r only; Eq. (4) becomes

$$\nabla^2 a_{1z} - a_{1z}/\lambda^2 = 5\langle 0|\mathbf{c}\cdot\nabla|1\rangle a_0/c^2\tau_N$$

which has the solution

$$a_{1z}(r) = c_1 J_0(ir/\lambda) - \tau_z\langle 0|\mathbf{c}\cdot\nabla|1\rangle a_0.$$

If we require that the heat current is zero at the walls, $a_{1z}(R)=0$ and c_1 may be determined.[14] It is found that

$$a_{1z}(r) = \tau_z\langle 0|\mathbf{c}\cdot\nabla|1\rangle a_0 g(r),$$

where $g(r) = 1 - J_0(ir/\lambda)/J_0(iR/\lambda)$. Thus

$$Q_z(r) = \lambda_z(C_v T/3\hbar)a_{1z}(r) \qquad (5)$$

and the definition of the inner product and the relation between a_0 and the local energy density yield

$$\lambda_z(C_v T/3\hbar)\langle 0|\mathbf{c}\cdot\nabla|1\rangle a_0 = \tfrac{1}{3}c^2(\partial\epsilon_T/\partial z).$$

For a steady heat current along the z axis we have $(\partial\epsilon_T/\partial z) = -C_v(\partial T/\partial z)$. Hence, Eq. (5) reduces to

$$Q_z(r) = -\tfrac{1}{3}C_v c^2\tau_z g(r)(\partial T/\partial z).$$

The thermal conductivity of the cylindrical lamina of radius r is

$$\kappa(r) = \tfrac{1}{3}C_v c^2\tau_z g(r) = \kappa_z g(r). \qquad (6)$$

The thermal conductivity is thus given by the Ziman limit κ_z multiplied by a geometrical factor $g(r)$ which embodies all effects due to flow pattern in a finite sample.

When $\tau_z \to +\infty$, $g(r) \to 5(R^2-r^2)/4c^2\tau_N\tau_z$ and τ_z drops out of Eq. (6) which reduces to the result of Sussmann and Thellung.[3] When $R \gg \lambda$, the solution of Eq. (5) has the asymptotic form $e^{-r/\lambda}$ and $g(r)$ becomes

$$g(r) \simeq 1 - \exp\{-(R-r)/\lambda\}. \qquad (7)$$

The heat current then differs from the prediction of the Ziman limit only within a mean free path of the boundary. In Fig. 1 we plot $g(r)$ versus R for typical values of R and λ for solid He^4 at 19.5 cm³/mole.

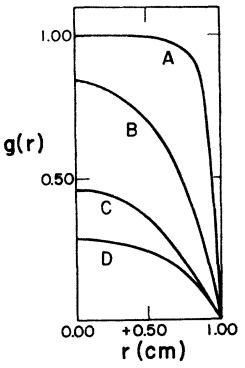

FIG. 1. The geometrical factor $g(r)$ as a function of r. Curves A–D are plots of $g(r)$ in the particularly sensitive region near the thermal-conductivity maximum: curve A, $T=0.76°K$, $\lambda=0.10$; curve B, $T=0.68°K$, $\lambda=0.30$; curve C, $T=0.64°K$, $\lambda=0.60$; curve D, $T=0.62°K$, $\lambda=1.0$. The value of $g(r)$ at $r=0$ is $g(0)=R^2/4\lambda^2$ for $\lambda \gg R$.

The averaged thermal conductivity across the sample is

$$\kappa = (\kappa_z/\pi R^2)\int_0^R 2\pi r g(r)dr = \kappa_z G(\mu), \qquad (8)$$

where

$$G(\mu) = 1 - 2J_1(iR/\lambda)/(iR/\lambda)J_0(iR/\lambda). \qquad (9)$$

$G(\mu)$ is a natural function of R and λ in the form $R^2/4\lambda^2 = \mu$. A plot of $G(\mu)$ as a function of μ is shown in Fig. 2. In the limit $\mu \ll 1$, $G(\mu)$ approaches zero as $\mu/2$. In the limit $\mu \gg 1$, $G(\mu)$ approaches 1 as $1-1/\sqrt{\mu}$. Rapid variation of $G(\mu)$ with μ occurs for $\mu < 1$. In the limit $\mu \ll 1$ the thermal conductivity given by Eq. (8) is

$$\kappa = \kappa_z \lim_{\mu\to 0} G(\mu) = \tfrac{1}{3}C_v c^2(5/4)R^2/c^2\tau_N \qquad (10)$$

in agreement with the result of Sussmann and Thellung and of Gurzi for Poiseuille flow of a phonon gas.

This experimentally effective thermal conductivity, Eq. (10), is understood by the following argument; the heat current carried by a phonon gas is proportional to

$$N(\mathbf{q})N_0 = \tau(\mathbf{q})\mathbf{c}\cdot\nabla T\partial N_0/\partial T, \qquad (11)$$

where the relaxation time $\tau(\mathbf{q})$ is the average lifetime for *momentum* in state $\mathbf{q}$. When $\lambda_N \ll R$ and $\lambda_R \gg R$, the principal mechanism for momentum loss is collision at the walls of the sample. However, the phonons do not fly directly to the walls as in the Casimir theory where $\tau(\mathbf{q}) \simeq R/c$, they diffuse to the walls, taking an average time τ_D given by

$$\tau_D \simeq (R/\lambda_N)^2\tau_N = R^2/c^2\tau_N. \qquad (12)$$

When this time is inserted in Eq. (11) a thermal conductivity qualitatively like that of Eq. (10) results.

The fact that $G(\mu)$ is a function of the combination of variables $R^2/4\lambda_N\lambda_R$ is understood by arguing that in order for τ_D to be the relevant time for momentum loss it must be shorter than the time for momentum loss due to R processes in the bulk, i.e.,

$$\lambda_D = c\tau_D \simeq R^2/\lambda_N \ll \lambda_R. \qquad (13)$$

Inasmuch as this condition will play a critical role in discussing the experimental situation we re-emphasize

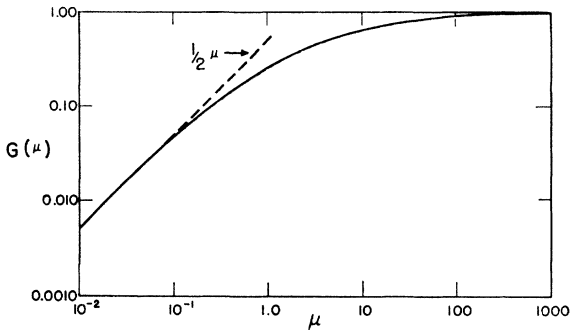

FIG. 2. The geometrical factor $G(\mu)$ as a function of μ.

by notation $\lambda_R \rightarrow \lambda_R{}^z$ that the R process mean free path is computed in the Ziman limit. Hence the combination of variables $R^2/4\lambda_N\lambda_R{}^z$ properly describes Poiseuille flow. This important condition cannot be obtained from Sussmann and Thellung.

Finally, the macroscopic equations employed in this discussion are valid only so long as $\lambda_N \ll R$, i.e., there is a sufficiently large number of phonon-phonon interactions to permit a macroscopic description over the cross section of the sample. Thus Poiseuille flow may contribute to the thermal conductivity only under the following conditions:

$$\lambda_N \ll R, \tag{14a}$$

$$\lambda_N \lambda^z{}_R \gg R^2. \tag{14b}$$

The notion of a Poiseuille flow window in the microscopic relaxation-rate spectrum is made explicit.

V. THERMAL CONDUCTIVITY (GENERAL)

We may use these results to generalize I(44), thus obtaining for the thermal conductivity:

$$\kappa = \tfrac{1}{3}C_v c^2[\langle 1|\tau_R{}^B|1\rangle(1-\Sigma)+\tau_z G(\mu)\Sigma], \tag{15}$$

where

$$\Sigma = 1/(1+s),$$
$$s = \langle 1|\tau_N|1\rangle/\langle 1|\tau_R{}^B|1\rangle,$$

and a boundary scattering augmented R-process rate has been defined to account for Casimir surface scattering as follows

$$(\tau_R{}^B)^{-1} = \tau_R{}^{-1} + \tau_B{}^{-1},$$
$$\tau_B{}^{-1} \simeq c/R.$$

In analogy with kinetic theory we now refer to the term $\langle 1|\tau_R{}^B|1\rangle$ in the bracket of Eq. (15) as the "kinetic term" and as noted before the term $\tau_z G(\mu)$ is called the "Ziman term." Equation (15) follows from I except for two important changes:

1. The switching factors are functions of τ_N and $\tau_R{}^B$ through the switching parameter $s = \langle 1|\tau_N|1\rangle/\langle 1|\tau_R{}^B|1\rangle$. The relaxation time which characterizes momentum loss, $\langle 1|\tau_R{}^B|1\rangle$, *includes* the Casimir boundary-relaxation time. This relaxation time naturally appears as the argument of the kinetic term when $\lambda_N \gg R$, i.e., $\tau_N \gg \tau_R{}^B$.

2. But the relaxation time which characterizes momentum loss processes when $\lambda_N \ll R$ is $\tau_R{}^{-1} = \tau_U{}^{-1} + \tau_I{}^{-1} + \cdots$; this summation of relaxation rates which gives τ_z in (15), *does not include* boundary relaxation τ_B. The boundary effect in the "Ziman term" resides in $G(\mu)$.

We believe Eq. (15) to be a necessary modification of I(44) or the usual Callaway expression for the purpose of analyzing thermal-conductivity data. It is simple to handle numerically, it is amenable to interpretation in terms of its two components, and becomes absolutely essential when Poiseuille phonon flow is a contributing factor.

The considerations of this section arose from our attempt to apply the Callaway method as in Ref. 7 to understand Poiseuille flow as discussed by Sussmann and Thellung. We exploit this generalization to discuss various experiments and show their interrelations.

In most cases the results we have obtained agree with those found independently by Gurzi.[4]

VI. TIME-DEPENDENT THERMAL CONDUCTIVITY

We found in I that the two sets of macroscopic equations lead to two distinctively different kinds of behavior for time-dependent thermal disturbances. In the limit that Eqs. (1a) and (1b) are valid the temperature obeys the Fourier heat law, Eq. (52) of I. An $\exp i(\mathbf{k}\cdot\mathbf{x}-\Omega t)$ temperature disturbance has the dispersion relation

$$-i\Omega+(\kappa/C_v)i\mathbf{k}\cdot i\mathbf{k}=0. \tag{16}$$

In the opposite limit, Eqs. (2a) and (2b) are valid, temperature obeys a propagating equation of motion, Eq. I(57), with the dispersion relation

$$k^2/\Omega^2 = (1/3c^2)(1-i\Delta), \tag{17}$$

where $\Delta = \frac{3}{5}\Omega\tau_N + [\tau_z G(\mu)\Omega]^{-1}$ measures the damping of the propagating temperature waves, second sound. The damping of second sound is due to second viscosity (the term $\Omega\tau_N$) and to the momentum loss scattering processes (the term $[\Omega\tau_z G(\mu)]^{-1}$). If second sound is propagated in a sample in which Poiseuille flow can occur the limiting momentum loss process is diffusion to the sample walls. The existence of Poiseuille flow considerably eases the restrictions on sample size for which second sound can be detected. This point is discussed further in the next section.

VII. DISCUSSION

A. Steady-State Measurements

There are four different temperature regions in which steady-state thermal-conductivity measurements can be accomplished. These are shown schematically in

Fig. 3. In Fig. 3: (1) the dashed curve 1 is the thermal conductivity given by the kinetic term of Eq. (15) alone without the switching factor; (2) the dashed curve 2 is the thermal conductivity given by the Ziman term alone without the geometrical factor $G(\mu)$ or the switching factor; (3) the dotted curve 3 is the thermal conductivity which results when the geometrical factor $G(\mu)$ is included in the Ziman term [thes witching factor is still not included]; (4) the solid curve is the expected measured thermal conductivity as a function of temperature, it is the superposition of the kinetic term and the Ziman term [including $G(\mu)$] with the appropriate switching factors.

In Fig. 4 we have plotted the various mean free paths which define the regions of Fig. 3. Above the temperature T_H at which $\lambda_N \simeq \lambda_R{}^B \simeq \lambda_U$, the kinetic term dominates the expression for the thermal conductivity; at intermediate temperatures, $T_L < T < T_H$, the N processes are relatively rapid compared to the R processes and the Ziman term dominates in Eq. (15); below the temperature T_L at which $\lambda_N \simeq \lambda_R{}^B \simeq R$ the kinetic term again dominates the expression for the thermal conductivity. The temperature T_m is the temperature at which the conventional thermal conductivity maximum occurs, $\lambda_U{}^z \simeq R$.

Region I (Casimir or Ballistic Region):
$\lambda_R{}^B \simeq R$, $\lambda_N \gtrsim R$; $T < T_L$

In this region the principal mechanism for momentum loss by the phonon gas is direct flight of the phonons to the boundaries of the sample. The Casimir boundary scattering theory gives the correct description of the phonon gas. The result of the Casimir theory is included in Eq. (15), through $\tau_B \simeq R/c$ in the kinetic term. Thermal-conductivity measurements in the ballistic region thus can yield information about specular and/or diffuse reflection at the boundaries as well as information about the crystallite size and quality of the sample being investigated. This latter information is particularly important in dealing with solid helium crystals. Because of their isotopic and chemical purity solid helium crystals may well become the proving ground for the basic ideas regarding the behavior of a phonon gas (see Ref. 15).

Region II (The Poiseuille Region):
$\lambda_N \ll R$, $\lambda_N \lambda_R{}^z \gg R^2$; $T_L < T < T_m$

These conditions are rather stringent and it is possible that a "window" does not exist, in which case regions I and III merge. But if region II exists the principal mechanism of momentum loss is diffusion to the boundaries of the sample. The thermal conductivity is given by the Ziman term of Eq. (15), including $G(\mu)$.

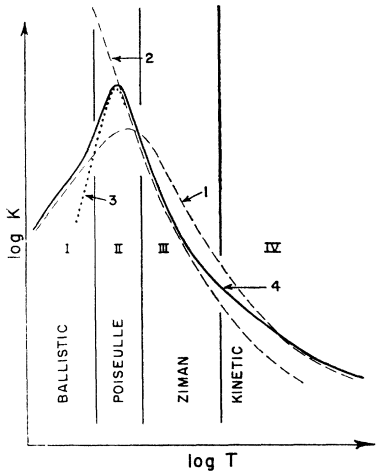

FIG. 3. Thermal conductivity as a function of temperature (see Sec. VI).

It is clear from Eq. (15) that in the absence of the Poiseuille flow window (i.e., for a sample in which the required inequalities cannot be satisfied) N processes make themselves known only through the switching factors. This relatively subtle influence is very hard to extract from the analysis of data. On the other hand we expect that if the Poiseuille region is observed free from the influence of the switching factors a clear-cut and simple measurement of τ_N results, Eq. (10). There is every reason to believe that the recent steady-state thermal-conductivity experiment by Mezov-Deglin[16]

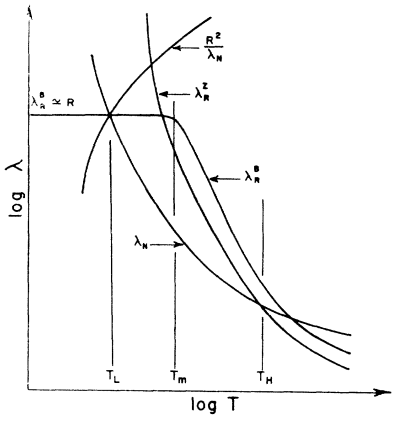

FIG. 4. The mean free paths as a function of temperature (see Sec. VI).

[15] The formal basis of the present development rests to an extent on treatment of the anharmonic interactions as "collisions." This is particularly implied when the terms "τ_N" and "mean free path λ_N" are used in the sense of time or space intervals between uncorrelated collisions. In strongly anharmonic materials like helium such a Markoffian treatment may not be valid. Nonetheless the conservation theorems on which the phenomena depend are of very general validity so that the effects discussed here probably will still occur. However, we note that the values of τ_N computed from the experiment of Mezov-Deglin on He^4 are of the same order of magnitude as a function of reduced temperature, T/Θ, as those found by Berman and Brock for LiF at the corresponding reduced temperature.

[16] L. P. Mezov-Deglin, Zh. Eksperim. i Teor. Fiz. **49**, 66 (1965) [English transl.: Soviet Phys.—JETP **22**, 47 (1966)]. Measurements of the thermal conductivity of carefully grown large crystals of solid He^4 show a very high thermal conductivity which varies as T^{7-8} below the maximum. This experiment definitely demonstrates Poiseuille phonon flow. This phenomena was suggested in earlier data of Mezov-Deglin, Zh. Eksperim. i Teor. Fiz. **46**, 1926 (1964) [English transl.: Soviet Phys.—JETP **19**, 1297 (1964)] and of M. Crooks, thesis, Yale University, 1962 (unpublished).

TABLE I. Steady-state experiments. For each of the regions discussed in the text, columns (a), (b), (c), and (d) show the microscopic scattering rates which define the region, the probable temperature range, the expression for the thermal conductivity in each region, and the relevant experiments, respectively.

Region	(a) Definition; microscopic parameters	(b) Temperature range	(c) Expression for thermal conductivity	(d) Experiments
I. (Ballistic)	$\lambda_N \gg R$, $\Sigma \to 0$ $\lambda_R \gg R$.	$T < T_L$ $T_L \simeq 0.015\Theta$	$\kappa = \frac{1}{3} C_v c^2 \alpha R/c$ $\alpha \simeq 1$	a Ref. 21
II. (Poiseuille)	$\lambda_N \ll R$, $\Sigma \to 1$ $\lambda_N \lambda_R{}^2 \gg R^2$. $\mu \ll 1$	$T_L < T < T_m$ $T_m \simeq 0.025\Theta$	$\kappa = \frac{1}{3} C_v c^2 (5/4) \dfrac{R^2}{c^2 \tau_N}$	Ref. 16
III. (Normal Ziman)	$\lambda_N \ll \lambda_R$, $\Sigma \to 1$ $\lambda_N \lambda_R{}^2 \ll R^2$. $\mu \gg 1$	$T_m < T < T_H$ $T_H \simeq 0.035\Theta$	$\kappa = \frac{1}{3} C_v c^2 \tau_z$	b Ref. 23 Ref. 19 Ref. 21
IV. (Kinetic)	$\lambda_N \gtrsim \lambda_R$, $\Sigma \to 0$ $\lambda_R \ll R$.	$T > T_H$	$\kappa = \frac{1}{3} C_v c^2 \langle 1 \vert R^{*-1} \vert 1 \rangle$	Ref. 19 Ref. 21

[a] R. Berman, E. Foster, and J. Ziman, Proc. Roy. Soc. (London) **A237**, 344 (1956); and P. Thacher, thesis, Cornell University, 1965 (unpublished).
[b] J. Callaway, Phys. Rev. **122**, 787 (1961).

accomplishes this and therefore is fundamentally more definitive than any other previous indirect measurements of τ_N.

Region III (The Ziman Normal Region): $\lambda_N \ll \lambda_R{}^2$, $\lambda_N \lambda_R{}^2 \ll R^2$; $T_m < T < T_H$

In this region the Poiseuille flow condition can no longer be met because of the increased rate of R-process scattering. The scattering centers distributed through the bulk of the sample now become the important mechanism for momentum loss. The thermal conductivity is given by the normal bulk Ziman term with $G(\mu) \simeq 1$. It is well known that the thermal conductivity given by the Ziman term can be substantially less than that given by the corresponding kinetic term due to the enhancement of the effectiveness of the R processes brought about by the rapid N processes. A measurement of the thermal conductivity in the extreme Ziman limit $\tau_N \to 0$ yields information about the flow component of the R-process scattering operator. Further, if the R-process scattering mechanism is strongly frequency-dependent the transition between III and IV will be pronounced.[17]

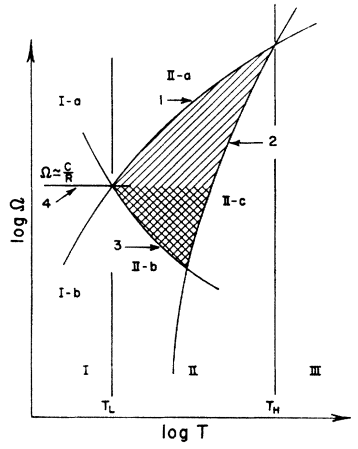

FIG. 5. The scattering frequency as a function of temperature. The conditions for second-sound propagation are fulfilled in the shaded region. The double cross-hatched part of the shaded region is the Poiseuille region when Ω is translated into mean free path.

Region IV (the Kinetic Region): $\lambda_R \ll \lambda_N \ll R$; $T > T_H$

In this region the principal mechanism of momentum loss continues to be the scattering distributed through the bulk of the sample. The kinetic term of Eq. (15) dominates. Measurement of the thermal conductivity in this region yields information about $\langle 1 \vert R^{*-1} \vert 1 \rangle$.

If we are dealing with an isotropically pure single crystal then this discussion must be modified somewhat. In a pure single crystal the only R process which exists at high temperature are the umklapp processes. The analysis of N and U processes at high frequencies is so complex that it is impossible to draw any general conclusion except that they are comparable in rate. Hence for a *pure* single crystal the limit corresponding to region IV may never be reached.

This discussion of steady-state measurements is summarized in Table I. In column (d) of that table we have indicated the experiments which we believe define the state of experimental knowledge about each region.

B. Time-Dependent Measurements

Time-dependent measurements can be made on heat pulses or continuous waves. The velocity of the waves and the distortion of their shape (due to dispersion and/or attenuation) are their most easily measured characteristics. The possible outcomes of heat-pulse measurements depend upon the temperature and its frequency of variation. We consider first an isotopically pure crystal. As with the case of steady-state measurements it is convenient to break up the temperature range into several regions. These are shown schemati-

[17] The conventional procedure for learning τ_N from a Callaway analysis of thermal-conductivity data depends upon the R-process scattering mechanism being frequency-dependent. If it is not, then the Ziman term is effectively indistinguishable from the kinetic term.

TABLE II. Time-dependent experiments. For each region discussed in the text, columns (a), (b), (c), and (d) show the microscopic scattering rate which defines the region, the probable temperature range, the quantity most easily extracted from measurements, and the relevant experiments, respectively.

Region	(a) Definition: microscopic parameters	(b) Temperature range	(c) Detected	(d) Experiments
I	$\lambda_R<\lambda_N$; $\Omega\tau_R\gg1$ $\Omega\tau_R\ll1$	$T<T_L$	energy velocity $\langle1\|R^{*-1}\|1\rangle$	Ref. 22
II	$\lambda_N\ll\lambda_R$; $\Omega\tau_R\ll1$. $\Omega\tau_R\gg1$ $\Omega\tau_R\ll1$, $\Omega\tau_R\lesssim1$ $\Omega\tau_R\gtrsim1$, $\Omega\tau_R\gg1$	$T_L<T<T_H$	second-sound velocity {τ_N or τ_z	...
III	$\lambda_N\gtrsim\lambda_R$; $\Omega\tau_R\lesssim1$ $\tau_R\lesssim\tau_N$	$T>T_H$	$\langle1\|R^{*-1}\|1\rangle$	a

[a] B. Abeles, G. Cody, and D. Beers, J. Appl. Phys. 31, 1585 (1960).

cally on Fig. 5 in which we have plotted the frequency of the various relaxation mechanisms as a function of temperature. In this figure curves 1, 2, 3, and 4 are the N-process scattering rate, the U-process scattering limit of τ_z, the effective momentum loss scattering rate $[\tau_z G(\mu)]^{-1}$ in the Poiseuille region, and the Casimir boundary scattering rate, respectively.

Region I: $\tau_R{}^B\simeq R/c\ll\tau_N$; $T<T_L$

In this region direct flight of phonons to the boundaries of the sample is the dominant mode of momentum loss, assuming diffuse scattering. Further the N processes are slow compared to the boundary-scattering processes. High-frequency pulses cannot thermalize (region I-a) and thus traverse the sample ballistically, as phonon bursts; low-frequency disturbances are strongly damped in much less than a wavelength (region I-b).

Region II: $[\tau_z G(\mu)]^{-1}\ll\Omega\ll\tau_N{}^{-1}$; $T_L<T<T_H$

The fundamental characteristic of this region is that everywhere the N-process scattering rate is faster than the effective R-process scattering rate. This is the second-sound region; it is shown shaded in Fig. 5. In this region heat pulses propagate as a superposition of second-sound waves. The dispersion relation, for these waves is given by Eq. (17). Detection of second-sound pulses will permit measurement of their velocities and attenuation. Second-sound pulses should propagate relatively undamped in the shaded region of Fig. 5. An experiment which sweeps Ω at fixed T and T at fixed Ω should be able to map out the boundaries of this region. The attenuation of high-frequency pulses $\Omega\tau_N\simeq1$ (along the upper boundary of the shaded region) is due to second viscosity, $\Omega\tau_N$, and measures τ_N; (region II-a). The attenuation of low-frequency pulses $\Omega\tau_z G(\mu)\simeq1$ (along the lower boundary of the shaded region) is due to R-process scattering. The existence of Poiseuille flow extends the second-sound region to lower frequencies than a Casimir restriction in the temperature range $T_L<T<T_m$. In this temperature range, low-frequency attenuation measurements should detect τ_N through the damping factor $(\Omega R^2/c^2\tau_N)^{-1}$, (region II-a). In the temperature range $T_m<T<T_H$ low-frequency-attenuation measurements detect $\langle1|R^*|1\rangle$, the Ziman limit of the R-process scattering operator (region II-c).

Measurements of second-sound attenuation should produce corroborative evidence for the results of Poiseuille-flow experiments.

Region III: $\lambda_N\gtrsim\lambda_R$, $\Omega\tau_R\lesssim1$; $T>T_H$

In this region the Fourier heat law is obeyed. Heat pulses propagate as a superposition of diffuse modes with the dispersion relation given by Eq. (16). Measurements on the velocity of diffusion and the attenuation yield information about $\langle1|R^{*-1}|1\rangle$.

The discussion we have given is modified in an obvious way if impurity scattering becomes important in the Ziman region.[18] In Fig. 6 we show the modification of Fig. 5 which results from a low concentration of impurities. The shaded region in this figure corresponds to the "new" second-sound region. The Ziman limit of the isotope-scattering rate now must be considered in the

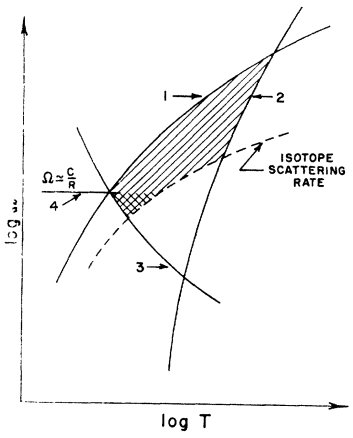

FIG. 6. The scattering frequency as a function of temperature. The conditions for second-sound propagation are fulfilled in the shaded region. The presence of isotope scattering in the Ziman limit severely restricts this region.

[18] Isotope scattering has about the same effective temperature dependence as N-process scattering. Hence if the two scattering mechanisms are at all comparable at some temperature they remain comparable at almost all temperatures (see Ref. 27).

condition $\Omega\tau_R \ll 1$; this condition becomes much harder to fulfill.

The results of this discussion of heat pulses are summarized in Table II. Again we have indicated [column (d)] the work which we believe defines the status of each experiment.

VIII. LiF and He^4

Recently a number of thermal-conductivity experiments have been performed and carefully analyzed. These analyses yield information which permits one to make quantitative statements about the various experiments discussed above.

A. LiF

Recently Berman and Brock[19] analyzed data on isotopic mixtures of LiF over a wide range of temperatures and concentrations. These authors found that the isotopic scattering strength predicted by Klemens[20] was entirely satisfactory and hence, by using the Callaway expression for the thermal conductivity were able to evaluate the strength of umklapp- and normal-process scattering with considerable confidence. We have taken the values of their parameters β_N and (β_U,a) and used them to compute the mean free paths; λ_N, $\lambda_U{}^z$, and $\lambda_I{}^z$ for a sample effective isotope concentration $x=0.001$, i.e., 0.1%, corresponding to the best LiF crystal of Thacher.[21]

Applying the criteria of the previous section we are then able to reach the following conclusions. (1) For the best presently available sample of LiF the optimum radius for an experiment to observe Poiseuille flow is $R\simeq 0.3$ mm. But even in such a sample Poiseuille flow should lead to a negligible contribution to the thermal conductivity. For Thacher's LiF sample with $x=0.001$ the maximum effective Poiseuille mean free path is $\simeq 0.09$ mm compared to a sample radius of $\simeq 0.3$ mm. Poiseuille flow will contribute only if the effective mean free path is larger than the sample radius.

The difficulty with the very excellent LiF crystals available is the still too large effective isotope concentration. The strongly frequency-dependent isotope scattering makes it impossible to get $\lambda_I{}^z$ large enough to satisfy the inequality $\lambda_I{}^z \gg R^2/\lambda_N$ required for Poiseuille flow. If the effective isotope concentration could be reduced by a factor of 10 the outlook for Poiseuille flow in LiF would be brightened.

We regard LiF as *typical* of a large number of solid samples in which thermal-conductivity measurements have been made. The failure of Poiseuille flow to be a well-known experimental phenomena is principally due to the imperfect condition of the crystals.

By contrast, the outlook for second-sound observation in LiF is not so dim. The conditions for propagation of second sound of wavelength $\lambda \simeq 2\pi c/\sqrt{3}\Omega$ are[7]

$$\lambda_N \ll \lambda,$$
$$\lambda_R{}^z \gg \lambda.$$

Using the numerical calculations discussed above we find that for a LiF sample of radius $R\simeq 2.0$ mm the effective mean free path for momentum loss at 20°K is 2.0 mm, i.e., $\lambda_R{}^z \simeq R \simeq \lambda$ whereas the N-process mean free path is $\simeq 0.2$ mm. The above inequalities are approximately satisfied in samples of presently attainable dimensions. Because of the impurity-scattering limitations in available LiF samples the absence of Poiseuille flow does not preclude the possibility of propagating second sound.

The failure of the experiments by Nethercot and von Gutfeld[22] to detect second sound could possibly be ascribed to the poor chemical condition of the samples investigated, but also the frequency and temperatures chosen were extremely unlikely to meet the required "window" conditions.[6,7]

B. He^4

Recently Bertman *et al.*[23] and Rogers *et al.*,[24] have measured the thermal conductivity of He^3-He^4 mixtures. Both of these groups have analyzed their measurements using the Callaway equation; they reached very different conclusions with regard to the strength of N-process scattering and lattice distortion scattering. We have again carried out the numerical calculations for isotopically pure, single He^4 crystals, using the parameters β_N and (β_u,a) from the analysis of both experiments, to obtain two sets of mean free paths: λ_N and $\lambda_U{}^z$ with which to examine the criteria for Poiseuille flow and second sound. The major quantitative difference in these two sets of mean free paths is in the N-process mean free path. Quantitative commentary on the possibility of Poiseuille flow and second sound is possible from these calculations.

However, there has been a fundamentally new experimental development in this whole subject, through the observation by Mezov-Deglin[16] of Poiseuille flow in single crystals of pure He^4. We believe that this experimental approach provides a direct method of measuring τ_N. *A priori*, then, τ_N obtained from a Poiseuille-flow experiment must be regarded as "directly measured "while that obtained from the conventional thermal-conductivity analysis is "indirectly determined," since τ_N is extracted in combination with many other quantities.

---

[19] R. Berman and J. Brock (to be published).
[20] P. G. Klemens, Proc. Phys. Soc. (London) **A68**, 1113 (1955).
[21] P. Thacher, thesis, Cornell University, 1965 (unpublished).
[22] R. J. von Gutfeld and A. H. Nethercot, Phys. Rev. Letters **12**, 641 (1964).
[23] B. Bertman, H. A. Fairbank, R. A. Guyer, and C. W. White (to be published).
[24] R. Berman, J. Rogers, and C. Bounds (to be published); hereafter this article is referred to as Rogers *et al.*, to distinguish it from Ref. 23.

TABLE III. Normal-process relaxation times. The normal-process relaxation times are computed from the results of the experiments of Mezov-Deglin (Ref. 16), Bertman *et al.*, (Ref. 23), and Rogers *et al.*, (Ref. 24).

T (°K)	(a) Mezov-Deglin (Ref. 16) (μsec)	(b) Bertman *et al.* (Ref. 23) (μsec)	(c) Rogers *et al.* (Ref. 24) (μsec)
0.5	1.0	1.2	0.05
0.6	0.7	0.5	0.02
0.7	0.4	0.2	0.01
0.8	0.3	0.1	0.007
0.9	···	0.06	0.004

Since our analysis is applicable to the Mezov-Deglin experiment we computed mean free paths λ_N from his results[25] for various conditions of pressure and temperature. Effective sound velocities and Debye temperatures were based on the results of Heltemes and Swenson.[26] The results for τ_N are given in Table III for a He^4 sample of about 19.5 cm^3/mole. Table III also shows the "indirectly determined" τ_N from Bertman *et al.*, and from Rogers *et al.*, for a similar sample. The discrepancies are apparent, so we comment further on this.

Bertman *et al.* chose τ_N to be of the form[27]

$$\tau_N^{-1}=\beta_N\omega^2T^3 \tag{18}$$

and found $\beta_N\simeq10^{-16}$ sec(°K)$^{-3}$. Rogers *et al.* chose τ_N with the somewhat milder temperature dependence

$$\tau_N^{-1}=\beta_N\omega^2T^2 \tag{19}$$

and found $\beta_N\simeq10^{-15}$ sec(°K)$^{-2}$. Hence at temperatures between 1 and 0.5°K the N-process mean free path from Eqs. (18) and (19) differ by a factor of 10 to 20. This difference would profoundly affect conditions for Poiseuille flow. In view of the greater significance of the direct measurement of τ_N, we regard the rather close agreement of Bertman *et al.* with Mezov-Deglin as of some interest, and at the same time can note that the discrepancies with Rogers *et al.* is typical of the large uncertainties characteristic in conventional analysis of thermal-conductivity data.

Note added in proof. Since the original preparation of this manuscript second sound has been observed in solid He^4 by Ackerman *et al.* [C. C. Ackerman, B. Bertman, H. A. Fairbank, and R. A. Guyer, Phys. Rev. Letters **16**, 789 (1966)].

[25] We estimate that for the 60- and 85-atm data of Mezov-Deglin, near the thermal-conductivity maximum, the effect of the kinetic term is less than 10%. Hence the raw data alone should yield a good approximation to τ_N.

[26] E. C. Heltemes and C. A. Swenson, Phys. Rev. **128**, 1512 (1962).

[27] Each ω in the expression for $\tau(\mathbf{q})$ leads to a T in the average of τ over the phonon spectrum. Hence, Bertman *et al.* have a τ_N proportional to T^{-5}; that of Rogers *et al.* goes as T^{-4}. These N-process power laws lead to T^8 or T^7 temperature dependence in the Poiseuille region. The experiment of Mezov-Deglin cannot distinguish between these. The experiment of Mezov-Deglin shows a dependence of τ_N on pressure in qualitative agreement with that found by Rogers *et al.*, i.e., as pressure increases, τ_N increases at fixed T/Θ. The solid is relatively less anharmonic as pressure increases.

ACKNOWLEDGMENTS

We gratefully acknowledge very fruitful discussion about many aspects of this paper with G. V. Chester, A. Thellung, and S. J. Rogers.

APPENDIX A

This Appendix contains a commentary on the application of the Callaway equation to the class of phenomena which are discussed in this paper.

The Callaway-Boltzmann equation is

$$DN(\mathbf{q})=\left(\frac{\partial}{\partial t}+\mathbf{c}\cdot\nabla\right)N(\mathbf{q})$$
$$=-\frac{1}{\tau_N}[N(\mathbf{q})-N_0(T+\delta T,\mathbf{\Lambda})]$$
$$-\frac{1}{\tau_R}[N(\mathbf{q})-N_0(T+\delta T,0)], \tag{A1}$$

where $N_0(T,\mathbf{\Lambda})=[\exp(\hbar\omega+\mathbf{\Lambda}\cdot\mathbf{q})/k_BT-1]^{-1}$. The lore of this equation is found in a number of recent articles.[7,12] The solution of this equation is easily developed from the form

$$N(\mathbf{q})=N_0(T,0)+u_0\left[-\frac{\delta T}{T}+\frac{\tau_c}{\tau_N}\mathbf{c}\cdot\mathfrak{\beta}\right]-\tau_cDN(\mathbf{q}), \tag{A2}$$

where $N_0(T+\delta T,\mathbf{\Lambda})$ has been linearized in deviation from $N_0(T,0)$, $u_0=\partial N_0/\partial x$, $x=\hbar\omega/k_BT$, $\mathbf{\Lambda}=\hbar c^2\mathfrak{\beta}$ and $\tau_c^{-1}=\tau_R^{-1}+\tau_N^{-1}$. The iterative solution of (A2) is

$$N(\mathbf{q})=N_0(T,0)+\mu_0[1-\tau_cD+\tau_cD\tau_cD+\cdots]$$
$$\times\left[-\frac{\delta T}{T}+\frac{\tau_c}{\tau_N}\mathbf{c}\cdot\mathfrak{\beta}\right]$$

or

$$N(\mathbf{q})=N_0(T,0)+u_0(1+\tau_cD)^{-1}\left[-\frac{\delta T}{T}+\frac{\tau_c}{\tau_N}\mathbf{c}\cdot\mathfrak{\beta}\right]. \tag{A3}$$

τ_cD appears as a natural expansion parameter for the solution. The various moments of Eq. (A1) with the solution (A3) lead to

$$\sum_q A(\mathbf{q})DN(\mathbf{q})=\sum_q A(\mathbf{q})(1+\tau_cD)^{-1}D$$
$$\times\left[-\frac{\delta T}{T}+\frac{\tau_c}{\tau_N}\mathbf{c}\cdot\mathfrak{\beta}\right] \tag{A4}$$

from the left-hand-side of (A1) and

$$\sum_q A(\mathbf{q})\left\{-\frac{1}{\tau_N}[N(\mathbf{q})-N_0(T+\delta T,\Lambda)]\right.$$
$$\left.-\frac{1}{\tau_R}[N(\mathbf{q})-N_0(T+\delta T,0)]\right\}$$
$$=\sum_q A(\mathbf{q})\left\{-\frac{1}{\tau_c}[(1+\tau_c D)^{-1}-1]\right.$$
$$\left.\times\left[-\frac{\delta T}{T}+\frac{\tau_c}{\tau_N}\mathbf{c}\cdot\boldsymbol{\beta}\right]\right\} \quad \text{(A5)}$$

from the right-hand-side; these expressions are equal except that, when the collision term (A5) is used to obtain a conservation law, in order to make the law consistent with that obtained from the drift term (A4) one higher order must be kept in the expansion of $N(\mathbf{q})$.

Equations (A4) and (A5) can be combined to obtain the conservation laws in the convenient form

$$\sum_q A(\mathbf{q})u_0\frac{\tau_c}{\tau_N}\left\{(1+\tau_c D)^{-1}D\left[-\frac{\delta T}{T}+\frac{\tau_c}{\tau_N}\mathbf{c}\cdot\boldsymbol{\beta}\right]+\frac{\mathbf{c}\cdot\boldsymbol{\beta}}{\tau_R}\right\}=0. \quad \text{(A6)}$$

We may use this equation to find the macroscopic equations which result from the requirement of energy and momentum conservation. The results are:

Energy Conservation

$$\sum_q \hbar\omega u_0\frac{\tau_c}{\tau_N}\left[\left\{\frac{\partial}{\partial t}-\tau_c\frac{\partial^2}{\partial t^2}-\tau_c(\mathbf{c}\cdot\boldsymbol{\nabla})^2\right.\right.$$
$$\left.+3\tau_c^2\frac{\partial}{\partial t}(\mathbf{c}\cdot\boldsymbol{\nabla})^2\right\}\left(-\frac{\delta T}{T}\right)$$
$$+\frac{\tau_c}{\tau_N}\left\{(\mathbf{c}\cdot\boldsymbol{\nabla})+2\tau_c\frac{\partial}{\partial t}(\mathbf{c}\cdot\boldsymbol{\nabla})\right.$$
$$\left.\left.+\tau_c^2(\mathbf{c}\cdot\boldsymbol{\nabla})^3\right\}(\mathbf{c}\cdot\boldsymbol{\beta})\right]=0. \quad \text{(A7)}$$

Momentum Conservation

$$\sum_q \hbar\mathbf{q}u_0\frac{\tau_c}{\tau_N}\left[\left\{(\mathbf{c}\cdot\boldsymbol{\nabla})+2\tau_c\frac{\partial}{\partial t}(\mathbf{c}\cdot\boldsymbol{\nabla})\right.\right.$$
$$\left.+\tau_c^2(\mathbf{c}\cdot\boldsymbol{\nabla})^3\right\}\left(-\frac{\delta T}{T}\right)$$
$$+\frac{\tau_c}{\tau_N}\left\{\frac{\partial}{\partial t}-\tau_c\frac{\partial^2}{\partial t^2}-\tau_c(\mathbf{c}\cdot\boldsymbol{\nabla})^2\right.$$
$$\left.\left.+3\tau_c^2\frac{\partial}{\partial t}(\mathbf{c}\cdot\boldsymbol{\nabla})^2\right\}(\mathbf{c}\cdot\boldsymbol{\beta})+\frac{\mathbf{c}\cdot\boldsymbol{\beta}}{\tau_R}\right]=0. \quad \text{(A8)}$$

These equations are consistent including terms of order $\gamma=\Omega\tau_c$; where Ω denotes the time dependence of δT and $\boldsymbol{\beta}$. It is quite possible that $\tau_c(\partial/\partial t)$ and $\tau_c(\mathbf{c}\cdot\boldsymbol{\nabla})$ are of different order. Then it is convenient to choose $\gamma=\Omega\tau_c$ and $\rho=\mathbf{k}\cdot\mathbf{c}/\Omega$ ($\mathbf{k}$ characterizes the space variation of δT and $\boldsymbol{\beta}$) as parameters to denote the order of the contribution of various terms in $N(\mathbf{q})$. In the second-sound region $\rho\simeq 1$ and γ alone may be used for ordering. In the region where the Fourier heat law is obeyed, $\rho\simeq\gamma^{-1/2}$ and the higher order $(\mathbf{c}\cdot\boldsymbol{\nabla})$ terms in these equations can be important.

All of the results obtained in the text can also be derived from Eqs. (A7) and (A8).

Comparison of Eqs. (A7) and (A8) with Eqs. (1a) and (1b) and (2a) and (2b) of the text lead to the following conclusion: The energy-conservation equation (1a) or (2a) is the same in both limits $R^*\to+\infty$ or $N^*\to+\infty$. All but the leading terms in Eq. (A7) are spurious. These terms are a consequence of the relaxation-time approximation to N^* in the Boltzmann equation not preserving the known properties of that operator. No doubt also a number of the terms in Eq. (A8) are also spurious. We strongly believe that the use of the Callaway equation or equivalently Eqs. (A7) and (A8) in all but the limiting cases, where it corresponds to Eqs. (1a) and (1b) and (2a) and (2b), can lead to erroneous conclusions.